[9] L. Courtois, B. Chiron, and G. Forterre, "Propagation dans une lame de ferrite aimantée. Application à de nouveaux dispositifs non réciproques à large bande," *Cables Transmission*, pp. 416–435, Oct. 1973.
[10] T. J. Gerson and J. S. Nadan, "Surface electromagnetic modes of a ferrite slab," *IEEE Trans. Microwave Theory Tech.*, vol. MTT-22, pp. 757–763, Aug. 1974.
[11] L. Courtois, "Propagation oblique des ondes électromagnétiques dans une lame de ferrite aimantée parallèlement à ses faces," *Electron. Fis. Apl.*, vol. 16, pp. 286–294, Apr./June.
[12] R. W. Damon and J. R. Eshbach, "Magnetostatic modes of a erromagnetic slab," *J. Phys. Chem. Solids*, vol. 19, p. 308, 1961.

The Edge-Guided-Wave Circulator

P. DE SANTIS AND F. PUCCI

***Abstract*—A complete study is presented on "edge-guided-wave" circulators (EGC). The fundamental physical principles which underlie EGC's operation are established and exploited to construct a broad-band circulator in the 8–12-GHz band. The performance data are compared to those of a "continuous tracking" circulator (CTC) and a traditional *Y*-junction circulator.**

I. INTRODUCTION

Since 1971 a number of people have become interested in fabricating a three-port symmetrical microwave integrated circuit (MIC) circulator based on edge-guided-wave (EGW) propagation [1]–[6]. This type of propagation in MIC circuits deposited on a substrate of magnetized ferrite was originally studied by Hines [1]. It is based on a transversal field displacement effect which concentrates the electromagnetic (EM) field at one of the edges of the strip conductor for one sense of propagation and at the other edge for the opposite sense of propagation. One of the most attractive characteristics of EGW is that it is extremely broad band [2]. Although in principle one may think of exploiting EGW in a number of nonreciprocal passive devices, from the very beginning it turned out that some difficulties existed in having these waves circulate along curved edges, and that magnetic losses drastically limited the bandwidths predicted by theory [4], [5]. More specifically, laboratory experiments evidenced that EGW propagation along curved paths was plagued by the existence of spurious-volume mode resonances. That was the main reason why efficient EGW broad-band isolators were readily constructed, whereas no broad-band EGW circulator has as yet appeared which could outperform the traditional *Y*-junction MIC circulators.

On the other hand, a significant step forward in the construction of broad-band MIC circulators was recently made with the discovery of the continuous tracking principle [7].

It is the purpose of this work to present a complete study on the EGW circulator (EGC) beginning by clearly stating what it is and how it compares to other broad-band MIC circulators. A theoretical analysis on EGW along curved edges will be subsequently introduced, which is of relevance in understanding the performance of the EGC.

Finally, the performance data of a three-port EGC will be presented and compared with those of other types of MIC broad-band *Y*-junction circulators.

Manuscript received July 31, 1974; revised November 27, 1974.
The authors are with the Research Department, Selenia S.p.A., Rome, Italy.

II. DEFINITION OF EGW CIRCULATOR

MIC *Y*-junction circulators consist of a circular junction, which is the nonreciprocal part of the device, connected to the three ports of the device by means of suitable impedance transformers [Fig. 1(a)]. Under these circumstances only the circular junction or a slightly larger region is required to be magnetically active; i.e., realized with magnetized ferrite (shaded area). The impedance transformers are deposited on an isotropic substrate. An EGC is constituted by a suitably shaped MIC circuit [see Fig. 1(b)] deposited on a magnetically active substrate; i.e., both in the central part and in the impedance transformers nonreciprocal action takes place. Therefore a peculiar characteristic of the EGC is that, at variance with other types of circulators, a lateral field displacement effect occurs in the impedance transformers. Note that in an EGC the coupling angle 2ψ is always $2\pi/3$. Furthermore, from Fig. 1(b) it is apparent that in the EGC, the distinction between circular junction and impedance transformers is a fictitious one and that a modal expansion in terms of Bessel's functions is no longer valid.

Under these circumstances a modal analysis of the EGC seems to be rather involved, and approximate analytical techniques applied to simplified models seem to be in order.

III. EGW PROPAGATION ALONG CURVED EDGES

In the absence of an exact solution for the boundary value problem associated with an EGC, some useful information can be gathered from the analysis of simplified models. Obviously, the most elementary model that one can think of is the curved edge of a semi-infinite strip conductor deposited on a ferrite substrate (Fig. 2). Such a geometry has already been studied by one of the authors [8] and here only those results which are of relevance to the study at hand will be reported.

With reference to Fig. 2, if a Z-independent EM field is assumed, TM_Z modal solutions are possible and all field components can be derived from the Z component of the electric field which is given by

$$E_Z(r,\theta) = AH_n^{(2)}(K_f r) \exp(\pm jn\theta) \tag{1}$$

$$K_f = \frac{\omega}{C}(\mu_{\text{eff}}\epsilon_f)^{1/2}. \tag{2}$$

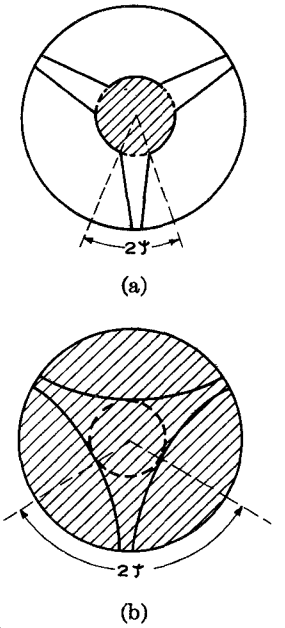

Fig. 1. Relevant to the definition of EGC. The shaded area represents the magnetically active region. $2\psi = 2\pi/3$ is the coupling angle.

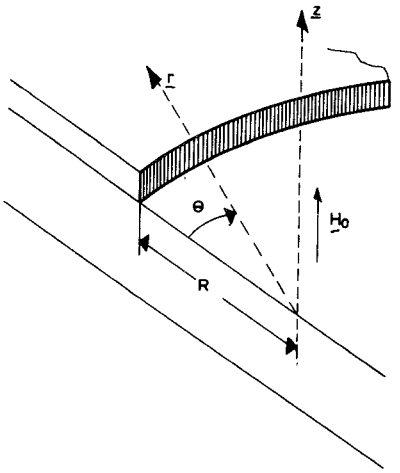

Fig. 2. The semiinfinite strip conductor with a circular guiding edge. R is the radius of curvature of the guiding edge.

Here A is an arbitrary amplitude constant, ω is the operation radian frequency, C is the velocity of light in vacuum, ϵ_f is the ferrite relative dielectric constant, $\mu_{eff} = (\mu_1^2 - \mu_2^2)/\mu_1$ is the equivalent relative magnetic permeability of the ferrite, μ_1 and μ_2 are the usual diagonal and off-diagonal components of Polder's tensor, $H_n^{(2)}$ is the Hankel's function of the second kind. From (1) and (2) one can appreciate how the behavior of the EM field in the ferrite region ($r > R$) depends upon the algebraic sign of μ_{eff}. When $\mu_{eff} < 0$, K_f is an imaginary quantity and the Hankel's function becomes a modified Bessel's function of the second kind. Under these circumstances the EGW propagates without radiation losses and n is a real quantity. When $\mu_{eff} > 0$, K_f is a real quantity, and n becomes complex; i.e., $n = n_1 + jn_2$ ($n_1^2 > 0$, $n_2^2 > 0$) due to radiation losses. In this case an attenuated EGW exists whenever $n_2 \ll n_1$. If perfect magnetic wall boundary conditions are applied at $r = R$, the following characteristic equation is found:

$$K_f R \frac{H_n^{(2)\prime}(K_f R)}{H_n^{(2)}(K_f R)} = \pm n \frac{\mu_2}{\mu_1} \tag{3}$$

which reduces to Hines' relation for $R \to \infty$. Here the prime indicates differentiation with respect to the argument.

In Fig. 3, $\hat{\omega} = \omega/\omega_i$ where $\omega_i = \gamma(H_0 - 4\pi M_s)$, γ is the gyromagnetic ratio, H_0 the applied dc magnetic field, $4\pi M_s$ the saturation magnetization, $\hat{R} = (R\omega_i/C\epsilon_f)$, $\hat{\omega}_m = [4\pi M_s/(H_0 - 4\pi M_s)]$, $\hat{K}_{\theta 1,2} = (n_{1,2}C\epsilon_f/R\omega_i)$, $\hat{\beta}_y = (\beta_y C\epsilon_f/\omega_i)$, $\beta_y = \lim_{R\to\infty}(n/R)$. An asymptotic solution of (3) for large R is found in [8] and is reported here for convenience

$$n_1 = \beta_y R + \frac{\mu_1}{2\,|\,\mu_2\,|} \tag{4}$$

$$n_2 = \beta_y R \left(\frac{\mu_2}{\mu_1}\right)^2 \exp\left[-2\beta_y R\left(\tanh^{-1}\frac{\mu_2}{\mu_1} - \frac{\mu_2}{\mu_1}\right)\right]. \tag{5}$$

These relations are plotted in Fig. 3 for a numerical case of interest. The principal result of the analysis is that whenever the guiding edge has a finite curvature and $\mu_{eff} > 0$, some energy is radiated from the edge into the ferrite volume. The amount of radiation increases as R decreases. This result has been experimentally checked [8]. At this point, the results obtained for a semiinfinite geometry must be transferred to a finite geometry of a real EGC.

This is done on an intuitive basis, being inspired by what happens in a similar situation: the radiation of a source in a finite region of space. Having in mind this situation, the radiation field associated with the leaky EGW is supposed to undergo a geometrical quantization due to the finite size of the "irradiated" region, and to set up volume wave modes in the "resonator" comprised between the RF

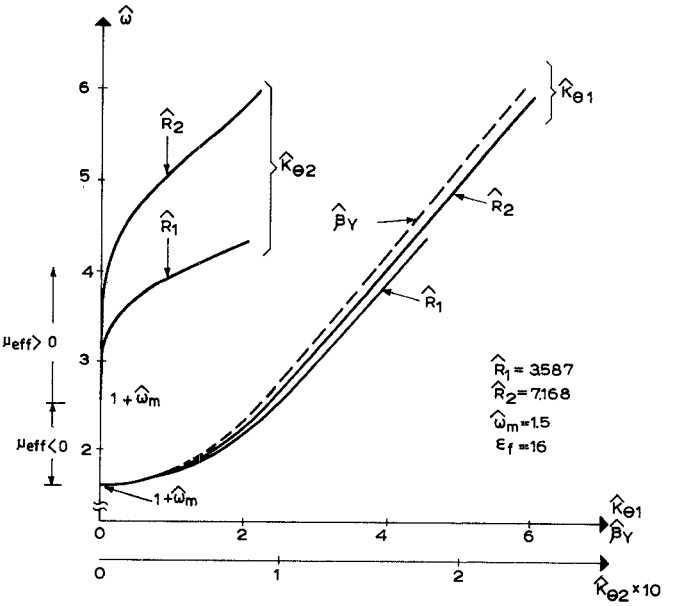

Fig. 3. Normalized Brillouin diagram for EGW along the circuit of Fig. 2. The ferrite is YIG and $H_0 = 3000$ Oe.

conductor and the ground plane. The conclusion is therefore drawn that if no volume wave resonances are to exist, either $R = \infty$ or $\mu_{eff} < 0$.

IV. THE PRACTICAL REALIZATION OF AN EGC

In this section the design and realization of MIC–EGC operating at X band over the frequency range 8–12.5 GHz is presented and compared to other broad-band MIC circulators. The ferrite substrate is YIG ($4\pi M_s = 1780$ Oe, $\epsilon_f = 16$, $\Delta H = 35$ Oe) produced in our laboratories. A preliminary specimen was fabricated on the basis of the experience gained in the construction of EGW isolators operating in the same frequency band. After some cut and try the final shape of the strip conductor was obtained as shown in Fig. 4. As predicted by theory no spurious resonances were observed under conditions of $\mu_{eff} < 0$. However, this condition is met only over a limited frequency range, i.e., $\alpha(H_0^2 - H_0 4\pi M_s)^{1/2} < (\omega/\gamma) < H_0$, where α is a number greater than unity which accounts for finite magnetic losses. If the bandwidth of the device is to be broadened, also $\mu_{eff} > 0$ conditions must be accepted and this means that suitable steps have to be taken in order to prevent spurious resonances.

We found that the most efficient means to kill unwanted ferrite volume modes is the use of a particular inhomogeneous magnetic bias.

In the light of the theoretical results obtained in the previous

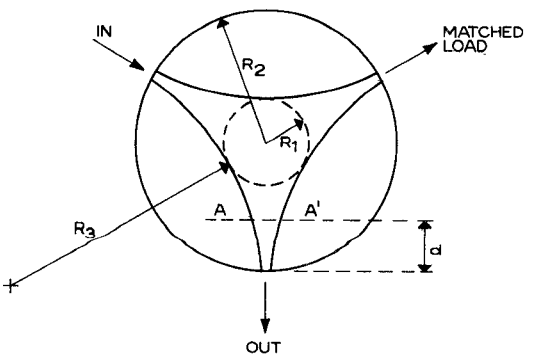

Fig. 4. Geometrical dimensions of the EGC operating at X band. In millimeters, they are $R_1 = 3.5$, $R_2 = 11$, $R_3 = 25$, $d = 7$.

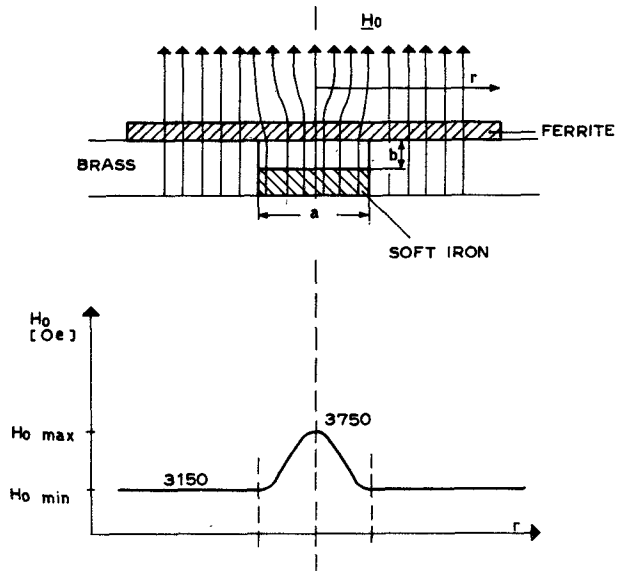

Fig. 5. The inhomogeneous magnetic bias used to suppress volume mode resonances. $a = 3$ mm, $b = 2$ mm.

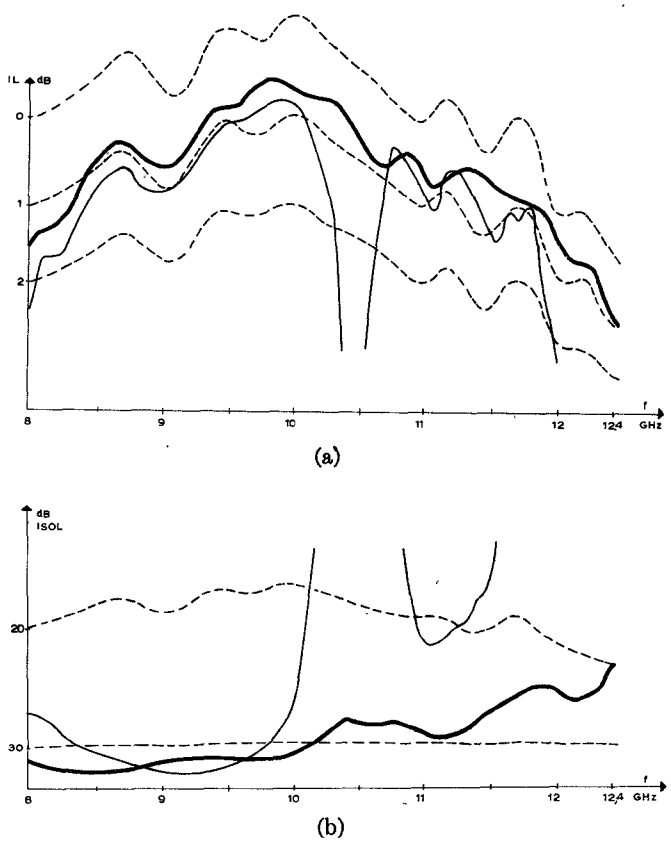

Fig. 6. (a) Insertion loss of EGC. The heavy solid line refers to an inhomogeneous bias with $H_{0,max} = 3750$ Oe and $H_{0,min} = 3150$ Oe. The thin solid line refers to a homogeneous bias of 3150 Oe. (b) Isolation of EGC. The same graphical notations as in Fig. 6(a) are used.

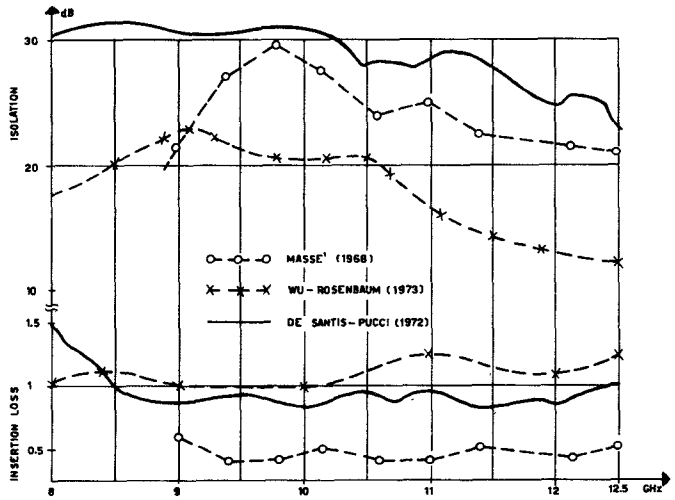

Fig. 7. Performance data of EGC, CTC, and Y-junction circulator at X band.

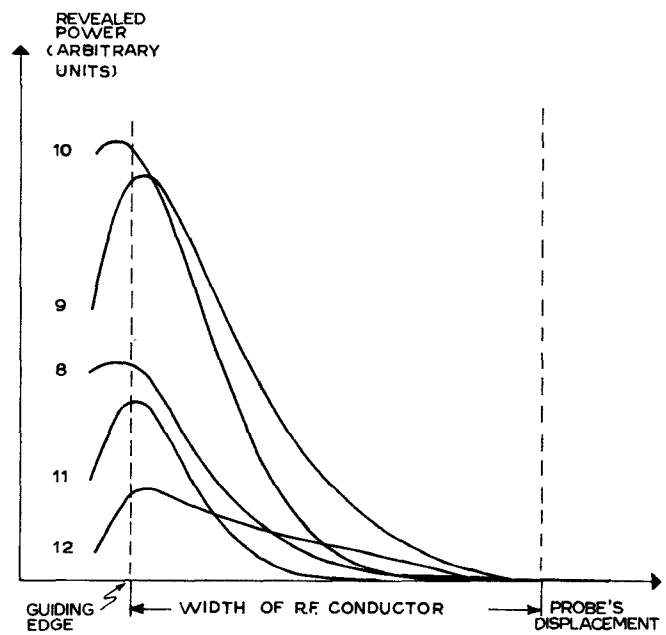

Fig. 8. Revealed power from a magnetic probe displaced along the line AA' of Fig. 4 under operation conditions. Frequencies are in gigahertz. The scale of displacement is 1:0.043.

section, we applied a dc magnetic field which would guarantee $\mu_{eff} < 0$ in the central region of the junction at those frequencies where volume wave resonances occur.

The practical realization of the magnetic bias is shown in Fig. 5. Experimental evidence was obtained that the optimal $H_{0,max}$ was 3750 Oe corresponding to a $\mu_{eff} < 0$ at the center of the junction for frequencies between $f_1 = 7.61$ GHz and $f_2 = 10.5$ GHz. Under these circumstances the magnetic losses associated with the resonant frequency f_1 are kept out of the operation band, while f_2 is sufficiently high to prevent the propagation of the volume wave-mode resonating at 10.47 GHz [Fig. 6(a) and (b)].

Fig. 7 shows the overall performance data of the EGC and compares them to those of some existing broad-band circulators such as the CTC [7] and the Y-junction circulator developed by Massé [9].

In order to demonstrate that the circulator described is in fact an EGC as defined in Section II, various measurements of the RF field spatial distribution were made by using both electric and magnetic probes. In particular, Fig. 8 shows a profile recorded by displacing a magnetic probe along the line AA' of Fig. 4, its loop being in the plane defined by the AA' line and the Z axis (scanning plane). These results, in conjunction with those obtained by using an electric probe parallel to H_0, and a magnetic probe with a loop perpendicular to the scanning plane, demonstrate unambiguously that under operational conditions a transversal field displacement effect is present in the AA' cross section of the taper. If $H_0 = 0$, this effect disappears and symmetrical profiles with respect to the taper's axis are found.

Note that the traditional $K_f R$ versus $|\mu_2|/|\mu_1|$ coordinate plane is not particularly suitable to represent the performance of the EGC, as it applies to a situation where μ_{eff} is greater than zero and space invariant.

V. CONCLUSIONS

A study has been made on the EGW circulator, which has led to the fabrication of a broad-band MIC circulator operating in the frequency range 8–12 GHz. The principal scope of the study was to establish the fundamental physical principles which underlie the EGC's operation and to show how they differ from those relative to the traditional Y-junction MIC circulators. It has been shown that broad-band operation of the EGC requires the introduction of mode-suppressing devices. Our choice was an inhomogeneous magnetic bias. Although the performance data of a three-port EGC favorably compare to those of other circulators, a greater complexity in mechanical construction as well as higher and more extended magnetic biases are necessary to guarantee a correct operation of the EGC. These are perhaps the principal reasons why such circulators as the continuous tracking circulator (CTC) will more likely enjoy the favor of microwave designers. For broad-band four-port circulators, the EGC version seems to be much more attractive mainly because no continuous tracking principle has been demonstrated to exist for this case [10]. The optimization of a four-port EGC is, however, still under way. The theory of the EGC seems to be at a rather early stage and still deserves some attention.

ACKNOWLEDGMENT

The authors wish to thank Dr. C. Misiano for the construction of the circulators.

REFERENCES

[1] M. E. Hines, "Ferrite phase shifters and multiport circulators in microstrip and strip line," in *Dig. of Tech. Papers, 1971 IEEE G-MTT Int. Microwave Symp.* (Washington, D. C.), pp. 108–109.
[2] ——, "Reciprocal and nonreciprocal modes of propagation in ferrite stripline and microstrip devices," *IEEE Trans. Microwave Theory Tech.*, vol. MTT-19, pp. 442–451, May 1971.
[3] ——, "Ferrite transmission devices using the edge-guided modes of propagation," in *Dig. of Tech. Papers, 1972 IEEE G-MTT Int. Microwave Symp.* (Chicago, Ill.), pp. 236–237.
[4] P. de Santis and F. Pucci, "Novel type of M. I. C. symmetrical three-port circulator," *Electron. Lett.*, vol. 8, pp. 12–13, Jan. 1972.
[5] ——, "Experiments on the optimization of a novel M. I. C. symmetrical three-port circulator," in *Dig. of Tech. Papers, 1972 IEEE G-MTT Int. Microwave Symp.* (Chicago, Ill.), pp. 238–240.
[6] M. Blanc, L. Dusson, and J. Guidevaux, "Etudes de dispositifs non reciproques a ferrite a trés large bande. Premieres realizations," *Rev. Tech. Thomson-CSF*, vol. 4, pp. 27–48, Mar. 1972.
[7] Y. S. Wu and F. J. Rosenbaum, "Wideband operation of microstrip circulators," in *Dig. Tech. Papers, IEEE G-MTT 1973 Int. Microwave Symp.* (Boulder, Colo.), pp. 92–94.
[8] P. de Santis, "Edge guided modes in ferrite microstrips with curved edges," *Appl. Phys.*, vol. 4, pp. 167–174, Aug. 1974.
[9] D. Massé, "Broadband microstrip junction circulators," *Proc. IEEE* (Lett.), vol. 56, pp. 352–353, Mar. 1968.
[10] W. H. Ku and Y. S. Wu, "On stripline four port circulator," in *Dig. of Tech. Papers, IEEE G-MTT 1973 Int. Microwave Symp.* (Boulder, Colo.), pp. 86–88.

Measurements of Intercavity Couplings

A. E. ATIA, MEMBER, IEEE, AND
A. E. WILLIAMS, MEMBER, IEEE

***Abstract*—This short paper describes the determination of couplings within a system of coupled cavities by measuring frequencies at which the phase of the input reflection coefficient is either 0° or 180°. A high degree of accuracy may be achieved and corrections can be made for finite cavity Q.**

Manuscript received September 19, 1974; revised December 23, 1974. This short paper is based upon work performed in COMSAT Laboratories under the sponsorship of the International Telecommunications Satellite Organization (INTELSAT). Views expressed in this short paper are not necessarily those of INTELSAT.

The authors are with the COMSAT Laboratories, Clarksburg, Md. 20734.

INTRODUCTION

Accurate determination of coupling between electrical cavities is required to design direct-coupled cavity waveguide bandpass filters. Bethe's [1] small-hole coupling theory, modified for larger slots by Cohn [2], gives dimensions which are approximately correct and normally sufficient for filter transfer functions having a small number of cavities and monotic out-of-band responses.

However, for bandpass filters which have real transmission zeros, more stringent specifications are imposed on the accuracy of the coupling values. Therefore, to realize this improved accuracy, it is desirable to have some method of measuring the coupling values within the assembled filter. This short paper describes the use of measurements of the input reflection coefficient phase from a short-circuited set of cavities to determine intercavity coupling. The accuracy is sufficient for successful tuning of such filters as the non-minimum-phase optimum-amplitude bandpass waveguide filter [3].

MEASUREMENT TECHNIQUE

A general lumped-element equivalent circuit for a system of n coupled cavities is shown in Fig. 1. All resonant cavities are tuned to a resonant frequency $\omega_0 = 1/(LC)^{1/2} = 1$ rad/s and have the same impedance, $Z_0 = (L/C)^{1/2} = 1\ \Omega$. Use of a narrow-band approximation makes it possible to describe the coupling between the cavities as an $n \times n$, symmetric, purely imaginary matrix jM, which is frequency independent near ω_0. The element M_{ij} is the coupling between the ith and jth cavities.

The input impedance $Z_{11}^{(n)}$ is given by

$$Z_{11}^{(n)} = \frac{\det\,(j\lambda I - jM_n)}{\det\,(j\lambda I - jM_{n-1})} \tag{1}$$

where M_{n-1} is the matrix resulting from the deletion of the first row and column of M_n, $\lambda = s + (1/s)$, $s = j\omega$, and I is the identity matrix. Therefore, the poles and zeros of $Z_{11}^{(n)}$ are the eigenvalues of M_{n-1} and M_n, respectively.

In practice the reflection coefficient $\rho^{(n)}$, which is equal to $[Z_{11}^{(n)} - R]/[Z_{11}^{(n)} + R]$, is the parameter which is most easily measured. It follows that the 0° and 180° phase positions of $\rho^{(n)}$ correspond exactly to the poles and zeros of $Z_{11}^{(n)}$. The measuring technique used exploits the fact that frequencies of the zeros and poles of the input impedance can be measured with a high degree of accuracy. Then the coupling values are computed from a knowledge of these frequencies and the way in which the cavities are coupled. Analytically, this problem is equivalent to determining the values of the elements of a real symmetric matrix M from a knowledge of its eigenvalues and the eigenvalues of one of its first-order minors. Explicit expressions for the coupling coefficients are presented for some cases of practical importance (i.e., $n = 2$, 3, and 4). Additionally, a method for computing the couplings in the general case of arbitrary n is also described.

Two Cavities ($n = 2$)

The condition for synchronous tuning of the cavities is

$$\omega_p - \omega_{z1} = \omega_{z2} - \omega_p \tag{2}$$

where $\omega_{z1,2}$ and ω_p are the angular frequencies of the zeros and pole of $Z_{11}^{(2)}$, respectively. Under this condition, the input impedance is given by

$$Z_{11}^{(2)} = j\frac{\lambda^2 - M_{12}^2}{\lambda}. \tag{3}$$

The zeros are at $\lambda_z = \pm M_{12}$, and the poles are at $\lambda_p = 0$.

It can be seen from this equation that coupling M_{12} can be computed by accurately measuring the zeros of $Z_{11}^{(2)}$. Fig. 2(a) is a typical polar plot of the locus of $\rho^{(2)}$ as a function of frequency. Since